ENVIRONMENT & HEALTH

Open Access

This article is licensed under CC-BY 4.0

pubs.acs.org/EnvHealth

Article

O_3 Increment from Prescribed Burns: Implications for Air Quality and Public Health in the Southeastern United States

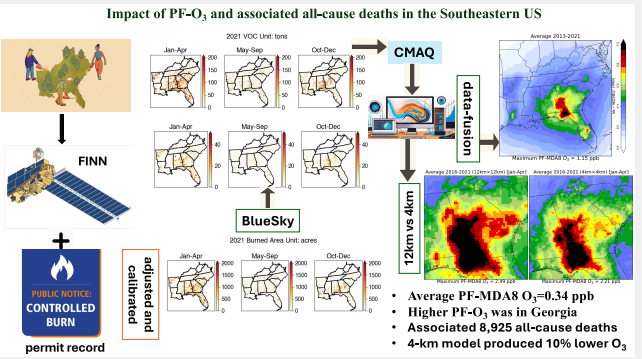
Kamal J. Maji, Zongrun Li, Yongtao Hu, Jennifer D. Stowell, Ambarish Vaidyanathan, Chad W. Milando, Gregory A. Wellenius, Patrick L. Kinney, Armistead G. Russell, and M. Talat Odman*

Cite This: https://doi.org/10.1021/envhealth.6c00221

Read Online

ACCESS | Metrics & More | Article Recommendations | Supporting Information

ABSTRACT: Prescribed fire (PF) is extensively practiced across the southeastern United States (US) to maintain fire-adapted ecosystems and reduce wildfire risk. However, PF emits substantial quantities of ozone (O_3) precursors that can elevate ground-level O_3 through photochemical reactions. This study quantified PF contributions to ambient O_3 and associated premature mortality across 12 southeastern US states from 2013 to 2021 using the Community Multiscale Air Quality (CMAQ) model at 12-km resolution. Model results were calibrated through data fusion with surface observations, and sensitivity to spatial resolution was examined with a nested 4-km simulation over Georgia. At 12-km resolution, contribution from PFs to daily maximum 8-h average O_3 (MDA8 O_3) concentrations averaged to 0.34 ± 0.12 ppb across the region, accounting for ∼0.9% of ambient levels. The PF contribution to daily maximum 1-h average O_3 (MDA1 O_3) averaged to 0.46 ± 0.18 ppb or ∼1.1% of ambient MDA1 O_3. At state level, highest annual average PF-MDA8 O_3 (0.59 ± 0.14 ppb) and PF-MDA1 O_3 (0.84 ± 0.22 ppb) were estimated in Georgia. Seasonal peaks (January−April) coincided with higher burning activity, with PF-MDA1 O_3 exceeding 1.0 ppb in Georgia, Alabama, Florida, and South Carolina. During the nine-year period, PF-related MDA8 O_3 exposure (short-term + long-term) associated 8925 (95% CI: 6273−11,567) premature all-cause deaths, with 62% linked to long-term exposure. Florida (2618), Georgia (1465), and North Carolina (910) experienced the highest absolute mortality burdens. The 4-km resolution model performed better than the 12-km model in estimating MDA8 O_3 concentrations. In Georgia, the 4-km simulation estimated approximately 10% lower PF-MDA8 O_3 concentrations and, consequently, approximately 10% fewer PF-MDA8 O_3-attributable premature deaths than the 12-km simulation. These findings highlight the regional health relevance of PF-related O_3 and underscore the need to integrate air-quality and public-health considerations into future PF management, particularly under climate-driven increases in fire activity.



KEYWORDS: *prescribed fire, air quality, ozone, premature deaths, resolution uncertainty*

1. INTRODUCTION

Decades of fire suppression policies in the United States (US) have led to substantial biomass accumulation in fire-adapted ecosystems, increasing the risk of high-intensity wildfires. This risk is being further amplified by climate change, which is lengthening fire seasons and exacerbating fuel dryness across much of the country.[1−3] Prescribed fire (PF)—the intentional, controlled application of fire under specific meteorological and fuel conditions—has become a central land management strategy to reduce wildfire hazard, improve forest resilience, and restore ecological processes disrupted by fire suppression.[4−6] While the western US has seen limited adoption due to topographic complexity, regulatory constraints, and narrow burn windows, the southeastern US has emerged as the national leader in PF implementation, accounting for approximately 70% of all prescribed burned area.[7−9]

In 2020, more than 38,000 km^2 were treated with PF nationwide, with 84% of that occurring on state and private lands. Notably, the southeastern US contributed nearly two-thirds of this activity, equivalent to ∼24,000 km^2 annually, and the burn area increased by 98% over the last 20 years.[10,11] Fire-prone ecosystems in this region, such as longleaf pine savannas and coastal plains, exhibit short fire return intervals, high fuel loads, and strong institutional and public support for burning as a landscape management tool. The air-quality impacts of PF have historically been studied primarily in relation to directly

Received: April 7, 2026
Revised: October 20, 2026
Accepted: October 21, 2026

ACS Publications

© XXXX The Authors. Co-published by Research Center for Eco-Environmental Sciences, Chinese Academy of Sciences, and American Chemical Society

Downloaded from pubs.acs.org/ehnea2/article-pdf/doi/10.1021/envhealth.6c00221/6901887/envhealth.6c00221.pdf by UNIV OF LYNCHBURG, Zongrun Li on 01 November 2026

emitted pollutants, particularly fine particulate matter ($PM_{2.5}$). PF smoke can substantially elevate ambient $PM_{2.5}$ concentrations near and downwind of burned areas, and previous studies have evaluated the resulting population exposure and associated respiratory and cardiovascular health impacts.[12,13] Consequently, smoke-management practices have focused on reducing exposure to $PM_{2.5}$ pollution.[14,15]

The scale and frequency of prescribed burning raise important questions regarding its influence on air quality, particularly concerning ozone (O_3), a secondary pollutant. O_3 is formed in the troposphere through photochemical oxidation of volatile organic compounds (VOCs) in the presence of nitrogen oxides (NOx) and solar radiation.[16,17] PF emits substantial quantities of NOx, nonmethane VOCs (NMVOCs), and radical-generating precursors such as carbon monoxide (CO), formaldehyde (HCHO), and nitrous acid (HONO).[18−20] These emissions can promote O_3 formation and the resulting O_3 production is inherently nonlinear and depends on the relative abundance of NOx and VOCs, plume age and dilution, solar radiation, temperature, meteorological conditions, and interactions between fire emissions and background anthropogenic and biogenic precursors. Consequently, the same quantity of PF precursor emissions may produce different O_3 responses depending on whether the surrounding atmosphere is predominantly NOx- or VOC-sensitive.[18−20]

Photochemical modeling studies have demonstrated that regional fire events can affect O_3, highlighting the importance of secondary pollutant formation. More recently, field studies in the southeastern US, conducted at Fort Moore (formerly and now Fort Benning), Georgia, have documented O_3 enhancements ranging from 5 to over 134 ppb following prescribed burns, occasionally contributing to exceedances of the US EPA National Ambient Air Quality Standard (NAAQS) for O_3, which is set at 70 ppb based on the annual fourth-highest daily maximum 8-h average O_3 concentration (MDA8 O_3), averaged over three consecutive years.[21] However, compared with $PM_{2.5}$, the regional-scale distribution and temporal variability of PF-attributable O_3 (PF-O_3) remain less comprehensively characterized.

Beyond PF's contribution to ambient O_3 concentrations, fire-derived O_3 may also have important public-health implications. Acute and chronic exposure to O_3 is linked to respiratory inflammation, exacerbation of asthma, reduced lung function, and increased mortality from cardiovascular and respiratory causes.[12,22] Previous health-impact assessments assumed equivalent health risks for wildland-fire and all-source O_3. Based on that assumption, an estimated 1332 all-cause deaths in the southeastern US were attributed to long-term exposure to PF-O_3 between 2013 and 2020.[23,24] However, recent evidence suggests greater health risks from wildland-fire O_3.[25] Therefore, quantifying PF-O_3 exposure using fire-specific epidemiological evidence is important for more accurately characterizing its potential health burden.

Our previous studies[23,24] quantified PF contributions to $PM_{2.5}$ and O_3 and their associated health impacts in certain sections of southeastern US states using forecast meteorology with ∼15% missing daily data. Those studies established the substantial contribution of prescribed burning to regional population exposure to $PM_{2.5}$ and, to a lesser extent, O_3. However, O_3 was considered alongside $PM_{2.5}$, and several aspects of PF-related O_3 remained unexplored. The present study focuses specifically on the formation and impacts of PF-attributable O_3. It extends the previous work by evaluating both daily maximum 1-h average O_3 (MDA1 O_3) and MDA8 O_3 across 12 southeastern states using hindcast meteorology during 2013−2021, characterizing spatial and seasonal variability and high-impact periods, quantifying both short- and long-term PF-MDA8 O_3-attributable mortality, and finally, evaluating the sensitivity of O_3 and health-impact estimates to 4-km versus 12-km model resolution in Georgia.[23,24] This study provides a comprehensive assessment of PF's contribution to O_3 pollution and associated health risks in the southeastern US and offers evidence to inform integrated strategies for fire management, air-quality protection, and public health.

2. METHODS

We designed a multistage modeling framework to estimate year-around PF-O_3 impacts on air quality in 12 southeastern US states (i.e., Alabama, Arkansas, Florida, Georgia, Kentucky, Louisiana, Mississippi, North Carolina, South Carolina, Tennessee, Virginia, and West Virginia). Specifically, we: (a) identified daily prescribed burned areas using the Fire INventory from NCAR (FINN) and calibrated them against burn permit records from 2013 to 2021; (b) estimated PF emissions using the BlueSky framework and simulated PF contributions to MDA1 O_3 and MDA8 O_3 metrics using WRF and CMAQ at 12-km resolution; (c) fused the simulated MDA1 and MDA8 O_3 fields with ground-based monitoring observations to improve accuracy; (d) utilized resulting PF-MDA8 O_3 estimates to quantify premature mortality associated with short-term and long-term exposures; (e) ran the same models at 4-km resolution over Georgia from 2016 to 2021 (with all other parameters held constant) to evaluate the impact of spatial resolution on model performance (Figure S1).

2.1. Prescribed Fire Emissions and Air-Quality Modeling

Prescribed burn permit records maintained by state agencies provide ground-based information on reported prescribed burned areas and can provide more accurate estimates of burn extent than satellite-derived products. However, the availability and completeness of these records were not consistent among the 12 southeastern states or across the entire study period.[26−29] Therefore, we used daily 1-km resolution burned-area information from FINN (version 2.5) to provide spatially and temporally consistent coverage across the study domain.[30] After applying the burn-type differentiation algorithm[31] to identify PFs, the FINN-derived daily prescribed burned areas were compared with available state daily permit records and adjusted using the reported daily burn information (i.e., location, date, and burned area). Although there was substantial variation in the difference between FINN burned areas and reported burn areas among the three states that provided permit records (Florida, Georgia, and South Carolina), we derived one calibration factor for all 12 southeastern states using all available data. This calibration was intended to correct the systematic overestimation of the prescribed burned area in FINN, resulting from its pixel-based, convex-hull aggregation of small, fragmented, and low-intensity fires.[32]

The adjusted burned areas were then incorporated into the BlueSky smoke modeling framework to estimate PF emissions.[33] BlueSky uses the Fuel Characteristic Classification System version 2 (FCCS) to estimate fuel loads at a 1-km resolution. To estimate emissions from combustion, BlueSky applies emission factors (EFs), which relate the mass of pollutants released to the mass of fuel consumed.[34] We implemented a coupled air-quality modeling system consisting of the WRF (version 3.9) for meteorological fields and CMAQ (version 5.4) for chemical transport.[35] In our framework, no fixed precursor-to-O_3 conversion factor was assumed; rather, PF-related O_3 emerged from the nonlinear atmospheric chemistry represented within CMAQ.

The modeling domain covered the southeastern US (23.71°−42.10°N, 95.30°−73.64°W) at a horizontal grid resolution of 12 km × 12 km, comprising 155 × 150 grid cells. To quantify the hourly

Downloaded from pubs.acs.org/ehnea2/article-pdf/doi/10.1021/envhealth.6c00221/6901887/envhealth.6c00221.pdf by UNIV OF LYNCHBURG, Zongrun Li on 01 November 2026

https://doi.org/10.1021/envhealth.6c00221
Environ. Health XXXX, XXX, XXX−XXX

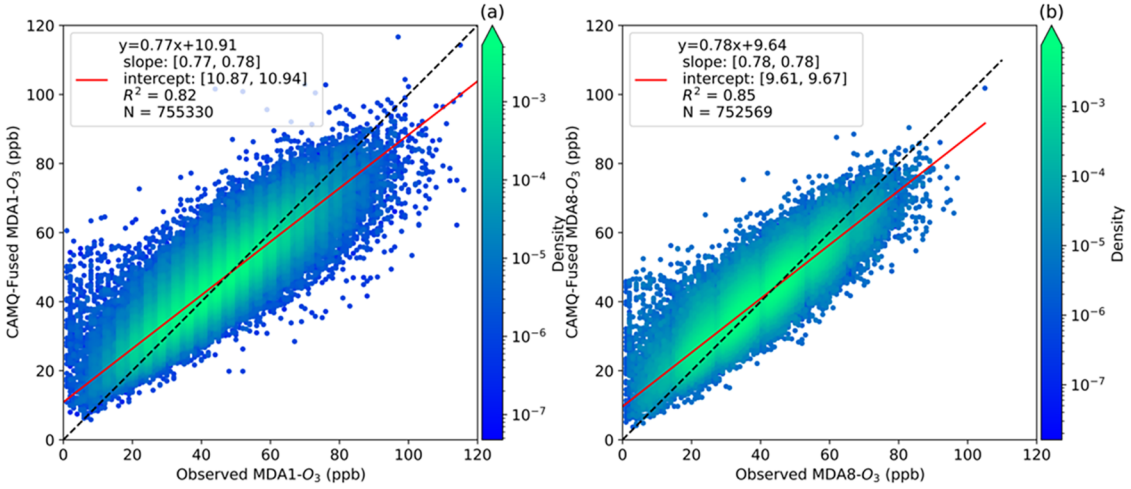


Figure 1. Density scatterplots of observed and 12-km data-fused model: (a) MDA1 O_3 and (b) MDA8 O_3 during 2013−2021. The dotted line shows 1:1.

contribution of PF to ground-level O_3 (PF-O_3), we conducted two CMAQ simulations for the period January 1, 2013, to December 31, 2021. The first simulation included all emission sources ($O_{3\text{-all}}^{sim}$) while the second excluded PF emissions ($O_{3\text{-no-PF}}^{sim}$). The PF-attributable O_3 concentration, PF-O_3^{sim}, was then calculated as the difference between the two simulations as

$$\text{PF-O}_3^{sim}(x, t) = \text{O}_{3\text{-all}}^{sim}(x, t) - \text{O}_{3\text{-no-PF}}^{sim}(x, t) \quad (1)$$

where superscript 'sim' indicates CMAQ-simulated concentration and 'x' and 't' denote space and time variability, respectively.

To evaluate the impact of model resolution on PF-O_3 concentration estimates, we applied the CMAQ model over a domain encompassing the state of Georgia (28.98°N, −87.82°W to 36.28°N, −79.13°W), using a 180 × 180 grid at 4 km × 4 km horizontal resolution for the period 2016−2021. All other model inputs and parameters were held constant across simulations to isolate the effects of spatial resolution. Simulated hourly O_3 concentrations were then postprocessed to calculate the MDA1 and MDA8 O_3 concentrations.

2.2. Data Fusion

Modeled concentrations differ from in situ measurements due to uncertainties of emissions inputs, meteorological parameters, and representations of nonlinear physical/chemical O_3 formation processes.[36,37] To reduce the model biases and error, we followed the method of Friberg et al.[38] and developed a more user-friendly method by Li et al.[37] for fusing observational MDA1 and MDA8 O_3 from Environmental Protection Agency's (EPA) Air Quality System (AQS) O_3 data with CMAQ results ($O_{3\text{-all}}^{sim}$). The observation data set contained 85.3 thousand MDA1 O_3 observations (306 sites) and 84.9 (304 sites) thousand MDA8 O_3 observations in 2013, which declined to 83.6 thousand (279 sites) and 83.5 thousand (279 sites), respectively, in 2021. The data fusion was conducted between CMAQ-simulated MDA1 or MDA8 O_3 and observed MDA1 or MDA8 O_3, using a polynomial regression model.[37] The resultant MDA1 or MDA8 O_3 concentration field ($O_{3\text{-all}}^{DF}$) leverages both temporal accuracies provided by observations and spatial completeness provided by CMAQ simulations. Finally, observation-adjusted PF-MDA1 or PF-MDA8 O_3 concentration fields (PF-O_3^{DF}) were generated by multiplying the simulated PF-MDA1 or PF-MDA8 O_3, (PF-O_3^{sim}) with the ratio of fused ($O_{3\text{-all}}^{DF}$) and simulated ($O_{3\text{-all}}^{sim}$) MDA1 or MDA8 O_3 concentrations as follows

$$\text{PF-O}_3^{DF}(x, t) = \text{PF-O}_3^{sim}(x, t) \times \frac{\text{O}_{3\text{-all}}^{DF}(x, t)}{\text{O}_{3\text{-all}}^{sim}(x, t)} \quad (2)$$

We aggregated the daily fused PF-MDA1 and PF-MDA8 O_3 concentration across the grids for individual counties, states, and the 12-state region using a weighted spatial mean approach. This was implemented using the '*exactextractr*' package in R 4.2.3.[39] The annual and seasonal means were then derived by averaging the daily means over the respective year or season.

The performance of the data-fusion method was evaluated separately for each year using 10-fold cross-validation (CV) with random observation-level withholding. The CV was not explicitly blocked by monitoring location or time; therefore, observations from the same monitoring site and/or time period could occur in both the training and validation data sets.

2.3. Premature Deaths Assessment

Although both PF-MDA1 and PF-MDA8 O_3 were evaluated in the air-quality assessment, only PF-MDA8 O_3 was used to quantify premature mortality. We selected MDA8 O_3 as the health-impact metric to reduce potential overestimation[40] and to maintain consistency with the exposure metric used in the epidemiological concentration−response relationships applied in this study.[41] To quantify premature deaths attributable to both short- and long-term PF-MDA8 O_3 exposures at the county level (x) and for each year (t), the data-fused PF-MDA8 O_3 concentrations and population-weighted exposure data were incorporated into eq 3. This analysis followed the well-established health-impact assessment method widely used in wildland-fire smoke exposure mortality studies[42−44]

$$\Delta\text{Mor}_{d,a}^{\text{PF-O}_3}(x, t) = \sum_{d,a} [(1 - \text{RR}_{d,a,\overline{\Delta\text{PF-O}_3^{DF}}})/\text{RR}_{d,a,\overline{\Delta\text{PF-O}_3^{DF}}}] \times B_{d,a}(x, t) \times \text{Pop}_a(x, t) \quad (3)$$

where d represents a specific disease (e.g., all-cause, cardiovascular etc.), while a denotes a specific age group, $B_{d,a}(x,t)$ is the baseline mortality rate (i.e., annual for long-term and daily for short-term mortality), and $\text{Pop}_a(x,t)$ is the age-specific population in the county. State-level mortality is obtained by summing $\Delta\text{Mor}_{d,a}^{\text{PF-O}_3}(x,t)$ for each county in each state within the study domain. $\text{RR}_{d,a}$ is the relative risk at annual average or daily average PF-MDA8 O_3 concentration.

Previous studies have typically assumed that the health risks attributable to O_3 from wildland fires are equivalent to those from all-source O_3 exposure.[24,45] However, recent epidemiological evidence suggests that O_3 generated from wildland-fire emissions may pose greater health risks.[41,46] While O_3 is the same molecule regardless of the source, we hypothesized that PF-O_3 could act as a tracer or proxy for different precursors or other pollutant mixtures within the smoke. Because specific epidemiological study estimates of mortality RRs to PF-derived O_3-attributable risk were not available, we applied RRs specific to wildland-fire-derived O_3 from Xu et al.[41] for both short- and long-term PF-MDA8 O_3 exposure and all-cause, cardiovascular, and respiratory mortality. We employed a log-linear concentration−

Downloaded from pubs.acs.org/ehnea2/article-pdf/doi/10.1021/envhealth.6c00221/6901887/envhealth.6c00221.pdf by UNIV OF LYNCHBURG, Zongrun Li on 01 November 2026

https://doi.org/10.1021/envhealth.6c00221
Environ. Health XXXX, XXX, XXX−XXX

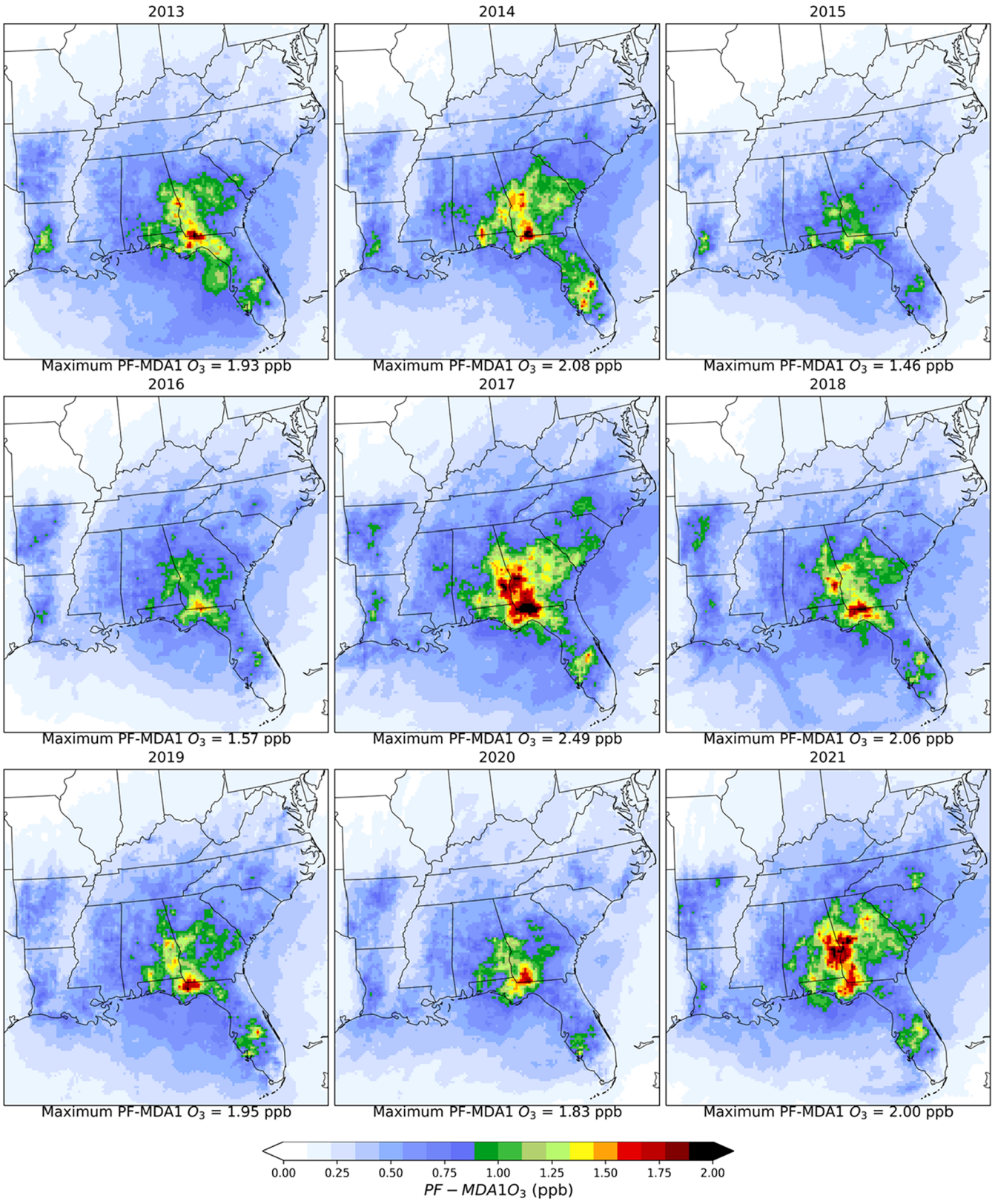


Figure 2. Spatial distributions of yearly average prescribed fire MDA1 O_3 concentrations (ppb) during 2013−2021.

response function (CRF) to estimate the RRs at the corresponding exposure concentrations (Tables S1 and S2).[44]

Long-term PF-MDA8 O_3-attributable mortality was estimated using the annual average county-level PF-MDA8 O_3 concentration. Short-term PF-MDA8 O_3-attributable mortality was estimated at the daily county levels during January−April, the peak PF-O_3 exposure season. Daily baseline mortality was estimated from the annual county-specific baseline mortality rate to calculate the number of deaths attributable to PF-MDA8 O_3 on each day. Daily attributable deaths were subsequently summed to obtain the annual short-term mortality.

https://doi.org/10.1021/envhealth.6c00221
Environ. Health XXXX, XXX, XXX−XXX

Downloaded from pubs.acs.org/ehnea2/article-pdf/doi/10.1021/envhealth.6c00221/6901887/envhealth.6c00221.pdf by UNIV OF LYNCHBURG, Zongrun Li on 01 November 2026

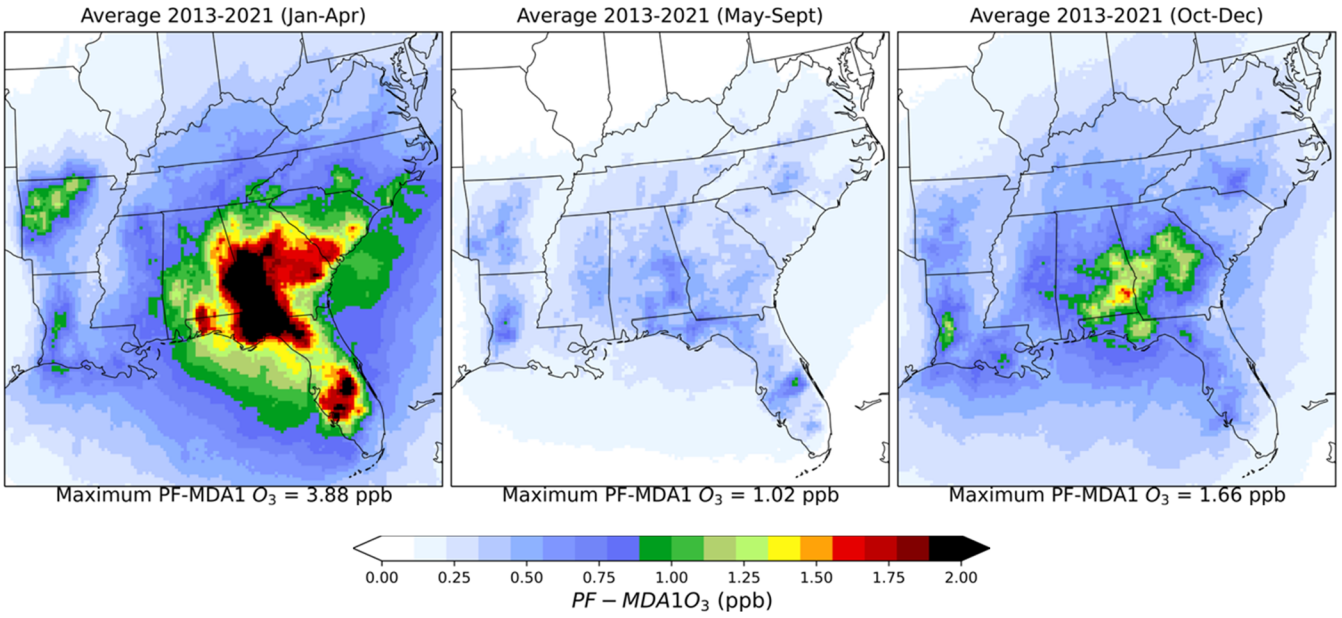


Figure 3. Spatial distributions of seasonal average prescribed fire MDA1 O_3 (ppb) during 2013−2021. January−April (left column) is the extensive burning season, May−September (center column) is the low burning season, and October−December (right column) is the moderate burning season.

Baseline mortality rates by specific year, county, disease, sex, and for individuals aged ≥25 years (i.e., age groups: 25−29, 30−34, 35−39, 40−44, 45−49, 50−54, 55−59, 60−64, 65−69, 70−74, 75−79, 80−84, and ≥85 years) were obtained from the Global Burden of Disease (GBD) results tool,[47] and corresponding county-level year and age-specific population data were sourced from the surveillance, epidemiology, and end results (SEER) database.[48] While GBD provided direct estimates of all-cause and cardiovascular mortality rates, it did not offer a standalone rate for total respiratory deaths. Therefore, in this study, we calculated respiratory mortality by aggregating the death rates for chronic respiratory diseases, lower respiratory infections, and upper respiratory infections.

3. RESULTS

3.1. Model Performances

The data-fused MDA1 and MDA8 O_3 estimates, which have been calibrated against monitoring station observations, showed much higher accuracy than MDA1 and MDA8 O_3 based purely on CMAQ simulation results (Table S3). Total MDA1 O_3 concentrations were slightly overpredicted by the data-fusion (DF) approach with a low mean bias (MB = 1.09 ppb) and a normalized mean bias (NMB = 2.5%). The DF method markedly improved the model performance for MDA1 O_3, achieving a higher coefficient of determination (R^2 = 0.82) across the study domain. Additional performance metrics further indicated enhanced accuracy, including a root-mean-square error (RMSE) of 5.07 ppb, normalized mean error (NME) of 8.7%, mean normalized bias (MNB) of 5.1%, and mean normalized error (MNE) of 10.4% (Figure 1). Similarly, total MDA8 O_3 concentrations were slightly overpredicted by the DF approach with an MB of 1.13 ppb and an NMB of 2.9%. The DF model also exhibited improved predictive capability, achieving a higher R^2 (0.85) and lower MNB (5.9%) and MNE (10.9%) compared to the base model (Table S3).

To further assess model robustness, a comprehensive 10-fold CV was conducted for each year, and the R^2 values in 10-fold CV of DF results against observations increased substantially from the nonfused results, from 0.50 to 0.78 for MDA1 O_3 and from 0.50 to 0.81 for MDA8 O_3, demonstrating the enhanced spatial and temporal consistency of the DF estimates. Furthermore, the averages of all 10-fold CV results satisfied the model performance criteria and goals recommended by Emery et al.[49] for the chemical transport model evaluation.

We ran our models at a 4-km resolution over Georgia from 2016 to 2021 (with all other parameters held constant) to evaluate the impact of spatial resolution on model performance. The results show that after DF, the 4-km resolution model outperformed the 12-km resolution model in estimating MDA8 O_3 concentrations. Specifically, the 4-km resolution model achieved an R^2 of 0.95, RMSE of 3.23 ppb, NMB of −2.7%, MNB of −0.63%, and MNE of 7%, compared to the 12-km resolution model's R^2 of 0.87, RMSE of 4.84 ppb, NMB of 5.7%, MNB of 9.7%, and MNE of 12.7% in Georgia (Table S4). Similar improvements were observed for MDA1 O_3 estimates in the 4-km resolution model than the 12-km resolution model in Georgia (Figure S6).

3.2. PF Ozone

The 2013−2021 average PF-MDA1 O_3 concentration in the 12 states was 0.46 ± 0.18 ppb (mean ± standard deviation), which accounted for 1.1% of ambient MDA1 O_3. There were significant differences in PF-MDA1 O_3 between the years: the Highest PF-MDA1 O_3 was estimated in 2017 (0.56 ± 0.22 ppb) and 2021 (0.52 ± 0.21 ppb), whereas the lowest PF-MDA1 O_3 was estimated in 2015 (0.40 ± 0.17 ppb) and 2020 (0.39 ± 0.15 ppb). At the state level, contribution of average PF-MDA1 O_3 was considerably higher in Alabama (0.7 ± 0.2 ppb), Florida (0.64 ± 0.27 ppb), Georgia (0.84 ± 0.22 ppb), and South Carolina (0.55 ± 0.1 ppb) (Figure S5 and Table S6). These levels accounted for ∼1.5−2% of ambient MDA1 O_3 in each respective state. Notably, Georgia experienced the highest annual average level of PF-MDA1 O_3, exceeding 1.0 ppb (2.4% of ambient MDA1 O_3) in 2017 and 2021. The highest average PF-MDA1 O_3 was estimated in Grady, Thomas, and Decatur counties in southwest Georgia and

Downloaded from pubs.acs.org/ehnea2/article-pdf/doi/10.1021/envhealth.6c00221/6901887/envhealth.6c00221.pdf by UNIV OF LYNCHBURG, Zongrun Li on 01 November 2026

https://doi.org/10.1021/envhealth.6c00221
Environ. Health XXXX, XXX, XXX−XXX

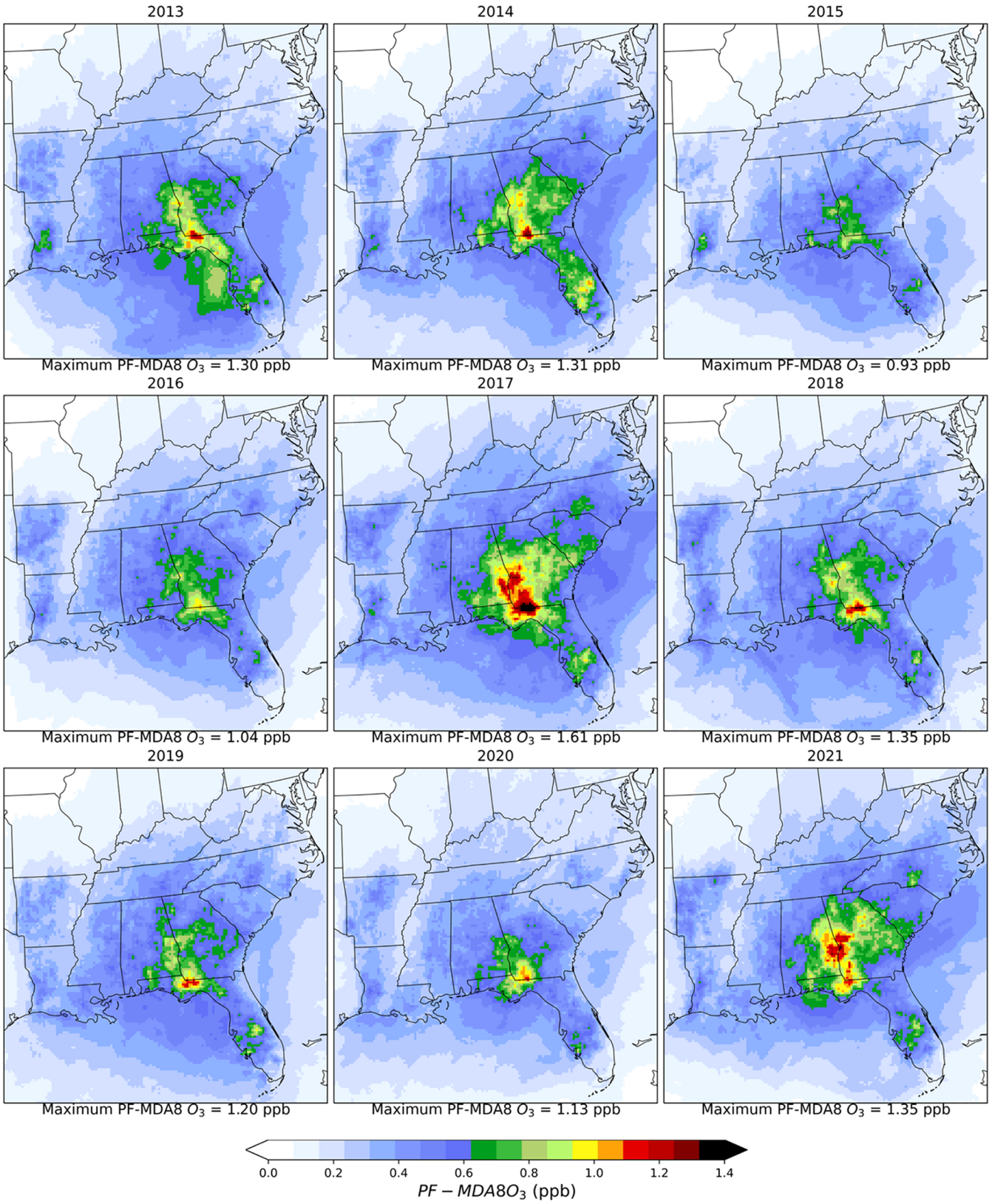


Figure 4. Spatial distributions of yearly average prescribed fire MDA8 O_3 concentrations (ppb) during 2013−2021.

Gadsden County in northwest Florida, reaching 1.4 ppb during 2013−2021 (Figure 2).

Seasonally, JFMA average PF-MDA1 O_3 concentration reached 0.73 ± 0.37 ppb (1.7% of the ambient MDA1 O_3) in the 12-state study domain and in Alabama (1.03 ± 0.34 ppb), Florida (1.17 ± 0.49 ppb), Georgia (1.54 ± 0.49 ppb), and South Carolina (1.03 ± 0.24 ppb), PF-MDA1 O_3 contributed ~2.7% to ambient MDA1 O_3 (Figure 3). Highest JFMA average PF-MDA1 O_3 was estimated in Georgia in 2017 (2.02 ± 0.74 ppb) and 2021 (1.82 ± 0.56 ppb). Average PF-

Downloaded from pubs.acs.org/ehnea2/article-pdf/doi/10.1021/envhealth.6c00221/6901887/envhealth.6c00221.pdf by UNIV OF LYNCHBURG, Zongrun Li on 01 November 2026

https://doi.org/10.1021/envhealth.6c00221
Environ. Health XXXX, XXX, XXX−XXX

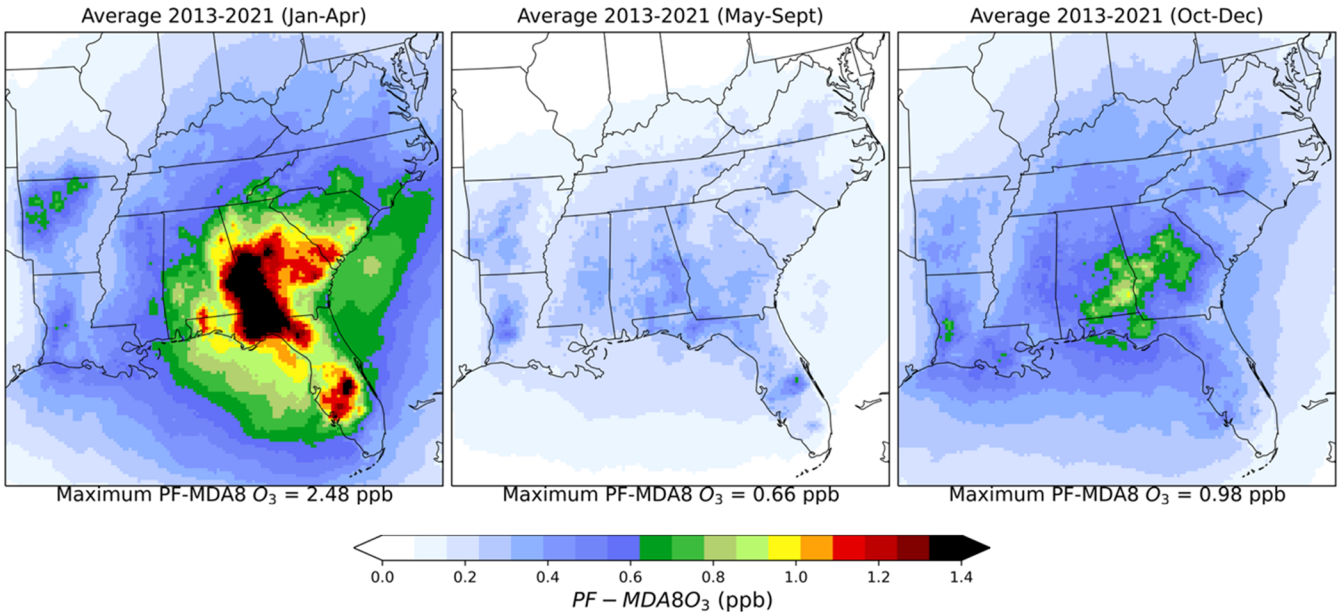


Figure 5. Spatial distributions of seasonal average prescribed fire MDA1 O_3 (ppb) during 2013−2021. The left column is during the January−April season, the center column is during the May−September season, and the right column is during the October−December season.

MDA1 O_3 was 0.26 ± 0.08 ppb during May−September (MJJAS) and 0.46 ± 0.1 ppb during October−December (OND), over the 12 states during the study period. During OND, average PF-MDA1 O_3 was 0.75 ± 0.22 ppb in Georgia and 0.77 ± 0.22 ppb in Alabama, accounting for ∼2% of the ambient MDA1 O_3 concentrations in these states (Figure S5). In 2014, 2017, 2020, and 2021, Georgia and Alabama recorded the highest average PF-MDA1 O_3 concentrations during the OND period (Tables S7−S9). In each of these years, more than 1,000 km^2 were burned during the OND season, contributing to the elevated O_3 levels. However, the total burned area during the JFMA period in Georgia and Alabama was considerably higher, reaching ∼13,700 km^2.

The average PF-MDA8 O_3 concentration across the study domain during the study period was 0.34 ± 0.12 ppb, accounting for approximately 0.9% of ambient MDA8 O_3 (Figure 4). In 2017 and 2021, the domain average PF-MDA8 O_3 exceeded 0.4 ppb. At the state level, the estimated 2013−2021 average PF-MDA8 O_3 concentrations were notably higher in Alabama (0.50 ± 0.11 ppb), Florida (0.45 ± 0.17 ppb), Georgia (0.59 ± 0.14 ppb), and South Carolina (0.41 ± 0.10 ppb) (Table S10). The Georgia average PF-MDA8 O_3 concentration was particularly high in 2017 (0.74 ± 0.20 ppb) and 2021 (0.70 ± 0.16 ppb). Grady, Thomas, and Decatur counties in southwest Georgia and Gadsden County in northwest Florida had the highest average PF-MDA8 O_3 levels of ∼1.0 ± 0.1 ppb during 2013−2021, accounting for about 2.5% of the ambient MDA8 O_3 in these areas.

During the JFMA period, average MDA8 O_3 concentrations increased by 0.53 ± 0.25 ppb over the study domain due to PF activity, accounting for ∼1.3% of ambient MDA8 O_3 during 2013−2021 (Figure 5). In comparison, average increases during MJJAS and OND were 0.20 ± 0.06 ppb and 0.34 ± 0.10 ppb, respectively. Notably, during JFMA, Alabama (0.74 ± 0.21 ppb), Florida (0.82 ± 0.31 ppb), Georgia (1.06 ± 0.30 ppb), and South Carolina (0.74 ± 0.15 ppb) experienced significant increases in PF-MDA8 O_3 across the study years. In 2017 and 2021, PF-MDA8 O_3 contributions during JFMA exceeded 2.5% of ambient MDA8 O_3 in these states (Tables S11−S13). Similarly, during OND in both 2017 and 2021, concentrations reached ∼0.70 ppb in Georgia and Alabama, contributing about 2% of ambient MDA8 O_3.

In each state, the highest PF-MDA1 and PF-MDA8 O_3 concentrations generally coincided with the periods of maximum statewide burned area. However, PF-O_3 levels are also influenced by prescribed burning activity in surrounding states and by prevailing meteorological conditions, such as wind speed, that govern smoke dispersion. For example, in Georgia, the highest PF-MDA1 and PF-MDA8 O_3 concentrations were observed on March 9 (12.3 and 9.3 ppb, respectively) and April 7 (12.1 and 9.3 ppb) in 2021. In contrast, lower values were observed on March 14, 2013 (4.5 and 5.9 ppb), despite a significantly larger burned area that day (167 km^2) compared to March 9 (104 km^2) and April 7 (82 km^2) 2021 (Figures S3 and S4). In 2020, the estimated PF-MDA1 and MDA8 O_3 concentrations in Alabama, Arkansas, Kentucky, Louisiana, Tennessee, and Mississippi were higher during OND compared to JFMA (Tables S11 and S113). This increase is attributable to a larger burned area in OND, which may have resulted from delays or restrictions on prescribed burning earlier in the year due to COVID-19-related limitations. Based on satellite-derived active fire data, fire activity in the southeastern US decreased by 21% during March−October 2020 due to COVID-19 compared to the 2003−2019 average for the same period.[50] During 2013−2021, at the state level, PF-MDA8 O_3 contribution exceeded 10% of the NAAQS for daily MDA8 O_3 (≥7 ppb) on 10 days in Georgia, 7 days in South Carolina, and 4 days in Alabama. However, these states experienced PF-MDA8 O_3 contributions accounting for ≥10% of ambient MDA8 O_3 on 45 days in Georgia, 17 days in South Carolina, and 15 days in Alabama.

At 4-km resolution, we estimated ∼10% lower annual average PF-MDA8 O_3 concentrations in Georgia compared to the 12-km resolution. For 2016−2021, the average PF-MDA8 O_3 concentration using 4-km resolution was 0.53 ± 0.12 ppb, compared to 0.59 ± 0.12 ppb estimated using 12-km

Downloaded from pubs.acs.org/ehnea2/article-pdf/doi/10.1021/envhealth.6c00221/6901887/envhealth.6c00221.pdf by UNIV OF LYNCHBURG, Zongrun Li on 01 November 2026

https://doi.org/10.1021/envhealth.6c00221
Environ. Health XXXX, XXX, XXX−XXX

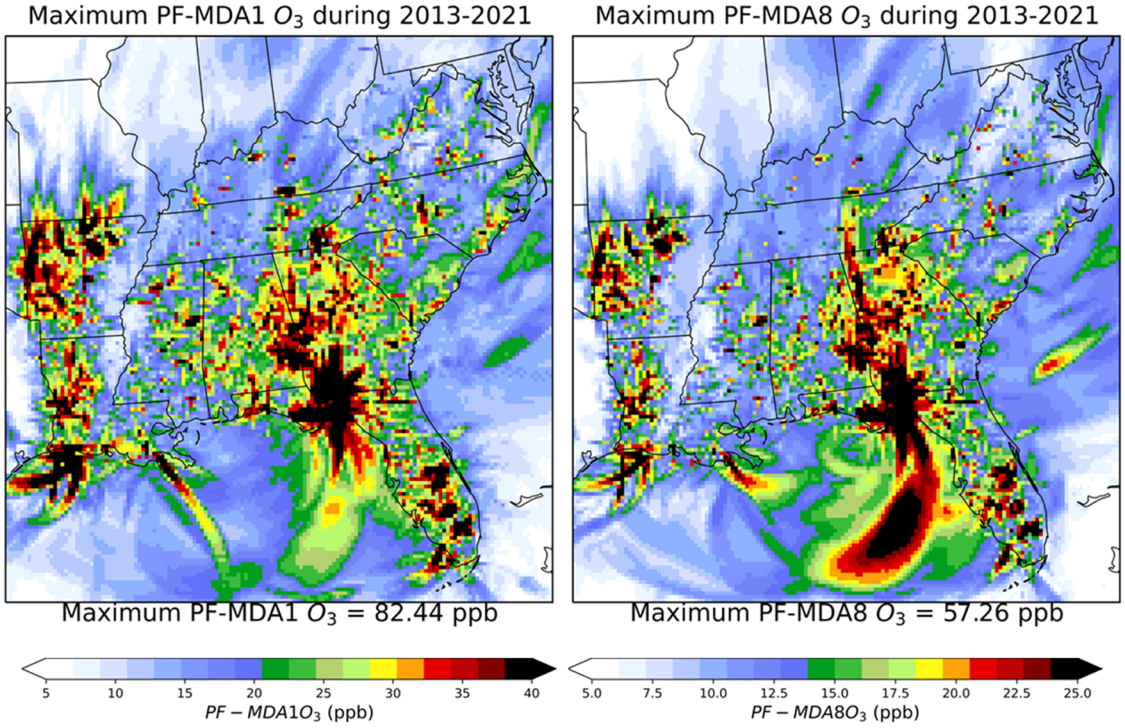


Figure 6. Grid maximum prescribed burn MDA1 O_3 (left) and MDA8 O_3 (right) during 2013−2021.

resolution. In 2017 and 2021, the annual average PF-MDA8 O_3 concentrations at 4-km resolution were 0.67 ± 0.18 and 0.65 ± 0.14 ppb, whereas at 12-km resolution, the estimated values were 0.74 ± 0.2 and 0.70 ± 0.16 ppb, respectively. Similar levels of lower PF-MDA8 O_3 concentrations were estimated with 4-km resolution during all seasons. In contrast, almost the same levels of annual average PF-MDA1 O_3 were estimated using 4-km (0.84 ± 0.21 ppb) and 12-km (0.83 ± 0.20 ppb) resolution in Georgia during 2016−2021. Using 4-km resolution, the highest annual average PF-MDA1 and PF-MDA8 O_3 concentrations were estimated in 2017, at 2.32 and 1.45 ppb, respectively. These values were lower than those estimated using 12-km resolution, with the highest annual averages for PF-MDA1 and PF-MDA8 O_3 of 2.49 and 1.61 ppb in 2017, respectively. The maximum PF-MDA1 and PF-MDA8 O_3 concentrations estimated using 4-km resolution were 68.7 and 46.7 ppb, respectively, approximately 20% lower than the corresponding maximum values of 82.4 and 57.3 ppb at 12-km resolution (Figure 6).

The annual and seasonal descriptive statistics for PF-MDA1 and PF-MDA8 O_3 concentrations (12-km model), including the mean, standard deviation (SD), median, and interquartile range (IQR), for each individual state are provided in Tables S6−S13.

3.3. Attributable Premature Deaths

In the 12 southeastern US states, an estimated total of 8,925 (95% CI: 6273−11,567) all-cause deaths were attributable to PF-related MDA8 O_3 exposure during 2013−2021 among the population aged ≥25 years. This includes 3213 (95% CI: 1348−5141) cardiovascular deaths and 1,208 (95% CI: 614−1796) respiratory deaths. These deaths attributable to PF-MDA8 O_3 exposure represented approximately 0.12%, 0.15%, and 0.20% of all-cause, cardiovascular, and respiratory deaths, respectively, across the 12 southeastern US states during the study period. The corresponding total premature mortality rates were estimated at 1.19 (95% CI: 0.83−1.53) per 100,000 residents for all-cause deaths, 0.43 (95% CI: 0.18−0.68) for cardiovascular deaths, and 0.16 (95% CI: 0.08−0.24) for respiratory deaths. Among the 8925 all-cause deaths attributable to PF-MDA8 O_3 exposure, 62% were linked to long-term exposure and 38% to short-term exposure, with the long-term to short-term death ratio ranging from 1.4 to 2.0 across the study period.

In 2017 and 2021, the estimated total all-cause deaths attributable to PF-MDA8 O_3 exposure were the highest, driven by elevated exposure levels, specifically, 1,156 (95% CI: 816−1496) and 1,426 (95% CI: 1006−1845) deaths, respectively. The highest numbers of total all-cause deaths (in nine years) attributable to PF-MDA8 O_3 exposure were estimated in Florida (2618; 95% CI: 1860−3373), Georgia (1465; 95% CI: 1037−1891), and North Carolina (910; 95% CI: 637−1181). However, when standardized per 100,000 population, the highest PF-MDA8 O_3-attributed all-cause mortality rates were observed in Alabama (1.74), Georgia (1.56), and South Carolina (1.42).

In Georgia, during 2016−2021, total estimated all-cause mortality (combined long- and short-term) attributable to PF-MDA8 O_3 using 4-km resolution was 963 (95% CI: 681−1244), approximately 10% lower than the estimate using 12-km resolution, which was 1,065 deaths (95% CI: 754−1374). The highest annual all-cause mortality in Georgia was estimated for 2021, with 244 deaths (95% CI: 173−314) estimated using 4-km resolution compared to 271 deaths (95% CI: 193−342) using 12-km resolution.

4. DISCUSSION

This study highlights the contribution of PF-attributable O_3 in the 12 southeastern US states, ranging from minor impacts on annual average concentrations to more pronounced effects on extreme burn days. Over the period 2013−2021, a total of

Downloaded from pubs.acs.org/ehnea2/article-pdf/doi/10.1021/envhealth.6c00221/6901887/envhealth.6c00221.pdf by UNIV OF LYNCHBURG, Zongrun Li on 01 November 2026

https://doi.org/10.1021/envhealth.6c00221
Environ. Health XXXX, XXX, XXX−XXX

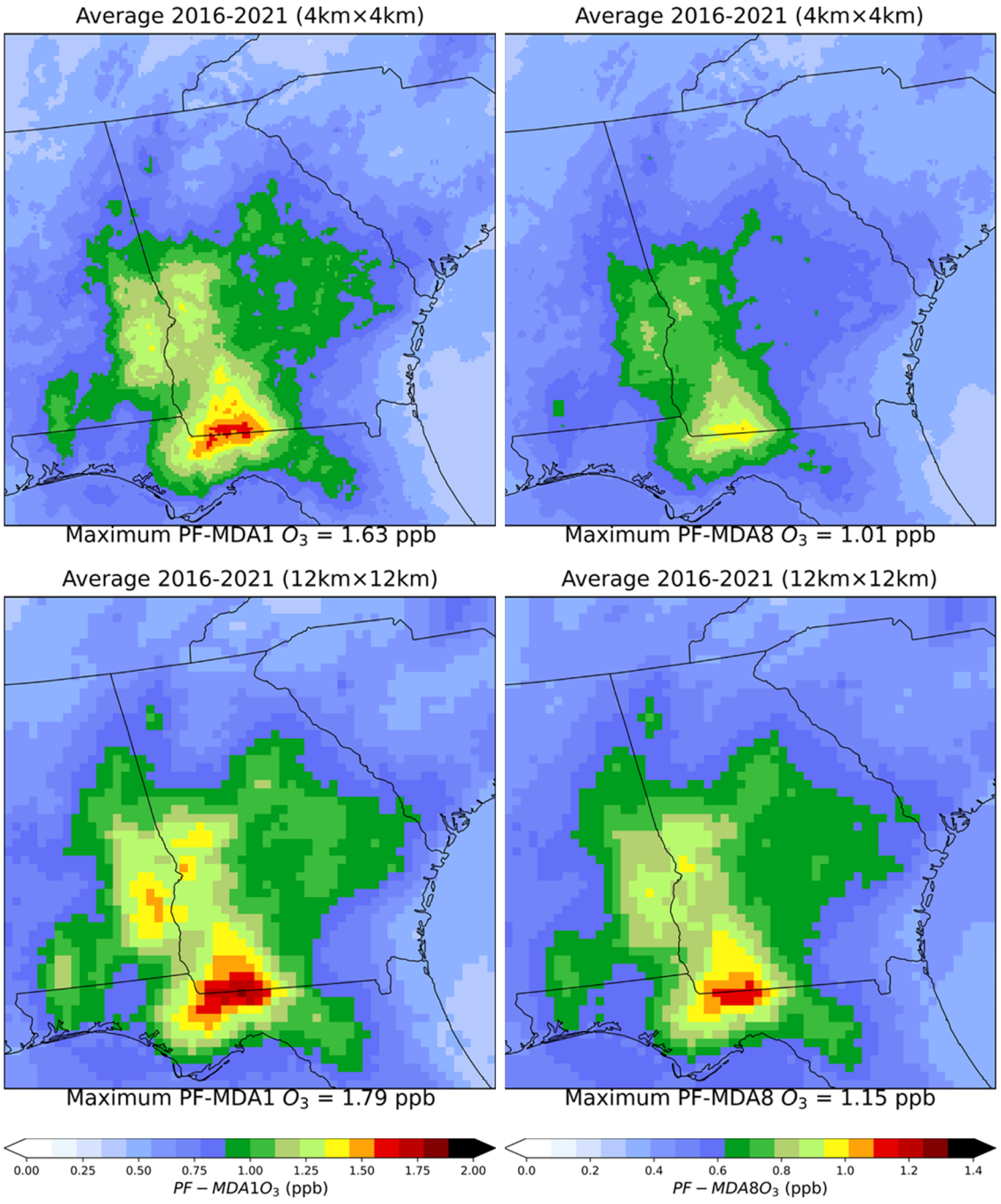


Figure 7. Prescribed burn MDA1 O_3 and MDA8 O_3 at 4 km × 4 km (top row) and 12 km × 12 km (bottom row) resolutions in Georgia and the surrounding area.

8925 all-cause deaths were attributable to PF-related MDA8 O_3 exposure. Our study offers several key advantages over previous works. First, we applied a burn-type differentiation algorithm to distinguish PF from other wildland fires in FINN and calibrated the resulting prescribed burned areas using available state permit records, improving the representation of PF activity. This calibration assumed uniform overprediction of burned areas by FINN in all 12 states, which is a potential source of uncertainty because there was substantial variation in overprediction among the three states that provided the permitted burn area records (Florida, Georgia, and South Carolina). Second, PF emissions generated using the BlueSky framework were integrated with WRF−CMAQ simulations, and the modeled O_3 fields were further constrained using ground-based observations through data fusion, substantially improving model performance. Third, the health-impact assessment applied wildland-fire-specific relative risks for both short- and long-term O_3 exposure rather than assuming equivalent toxicity to all-source ambient O_3. Finally, the comparison of 4-km and 12-km simulations in Georgia provided an explicit assessment of the influence of model spatial resolution on estimated PF-O_3 concentrations and associated mortality. Together, these features provide a comprehensive framework for characterizing the air-quality and public-health implications of PF-related O_3.

https://doi.org/10.1021/envhealth.6c00221
Environ. Health XXXX, XXX, XXX−XXX

Downloaded from pubs.acs.org/ehnea2/article-pdf/doi/10.1021/envhealth.6c00221/6901887/envhealth.6c00221.pdf by UNIV OF LYNCHBURG, Zongrun Li on 01 November 2026

We observed that the 4-km model outperformed the 12-km resolution model (Figure S6). However, the model resolution sensitivity analysis was conducted only in Georgia. Because PF-related O_3 impacts were not spatially uniform across the southeastern US, the sensitivity may not be the same for other states. Typically, the model performance is assessed by sampling the grid cell where an AQS monitoring site is located. However, AQS sites are unevenly distributed, concentrating in densely populated urban and suburban areas where O_3 levels are typically high rather than around prescribed burned areas. This uneven distribution introduces spatial bias when comparing coarse-resolution estimates to point-based measurements. Sampling 12-km resolution grids (144 km^2) over AQS site locations can result in significant biases due to spatial averaging effects.[51] The improved performance of the 4-km resolution estimates is largely due to the enhanced ability to capture spatial heterogeneities in O_3 precursor emissions, land use, and topography. At finer resolution, localized emission sources such as traffic corridors and industrial zones are more accurately represented, minimizing dilution that occurs with larger grid sizes.[52] Additionally, higher resolution better resolves terrain features and land cover variations that significantly influence meteorological drivers of O_3, such as wind flow, temperature gradients, and boundary layer dynamics. Consequently, this improves the representation of nonlinear chemical interactions, including O_3 titration by NO near emission sources and differentiation of NOx versus VOC-limited regimes.[53,54] These chemical processes are particularly relevant for PF plumes because O_3 production evolves as the plume ages and mixes with the surrounding atmosphere. Fresh plumes may contain sufficiently high NO concentrations to suppress O_3 locally through titration, whereas dilution and photochemical aging can subsequently promote net O_3 production as fire-emitted VOCs and NOx interact with background anthropogenic and biogenic precursors.[53]

In our previous work, the 4-km resolution model[23] yielded an annual mean PF-MDA8 O_3 concentration of 0.51 ppb for Georgia in 2017, while the 12-km resolution model[24] produced an estimate of 0.64 ppb. In the present study, the corresponding values rose to 0.67 ppb (4-km) and 0.74 ppb (12-km) (Figure 7). Two factors explain the higher estimates: first, the earlier analyses excluded ∼15% of days because of missing data, leading to a potential underestimation of annual means, and second, the current study employs the latest versions of WRF (v3.9) and CMAQ (v5.4), which offer improved meteorological inputs, updated gas-phase chemistry, and improved dry-deposition algorithms, thereby providing more accurate O_3 fields. Maji et al.[23] found that 4-km resolution modeling produced higher PF impact for $PM_{2.5}$ compared to 12-km resolution model outputs.[24] In contrast, for MDA8 O_3, the 4-km resolution simulations resulted in lower PF impact than those from 12-km resolution runs. This divergence is rooted in the fundamental atmospheric behavior of the pollutants: $PM_{2.5}$ is both a primary and secondary pollutant, while O_3 is a secondary pollutant. Primary $PM_{2.5}$ from prescribed burns, emissions from other local sources, terrain variability, and meteorological conditions are better resolved with fine resolution. Consequently, 4-km resolution models more accurately capture high-concentration plumes near fire sources that are diluted in coarser grids, resulting in elevated PF−$PM_{2.5}$ estimates.[55,56] Moreover, high-resolution models better simulate plume rise and diurnal emission timing, improving estimates of near-source $PM_{2.5}$ exposure.[57]

In contrast, most O_3 formation occurs downwind of prescribed burns through photochemical reactions and is sensitive to transport and chemical aging. Coarser models may overestimate O_3 production by overdiffusing fire plumes and artificially enhancing precursor mixing and photochemistry.[58] High-resolution models can resolve fine-scale dynamics such as NO titration near sources or within plumes, which can suppress O_3 formation and yield lower prescribed burn impact in the near field.[59,60] Grid size is especially important for PF-O_3 production, which involves nonlinear chemical reactions involving NOx and VOCs.[61,62] Jaffe et al.[14] emphasize that chemical transport models (CTMs) like CMAQ face substantial difficulty in reproducing wildland-fire-driven O_3. Biomass-burning plumes release large quantities of acetaldehyde, a key precursor to peroxyacetyl nitrate (PAN), which rapidly sequesters NOx, and accurate representation of this process hinges on both model grid resolution and the fidelity of emission inventories. When CTMs overestimate NOx and/or underestimate acetaldehyde, they routinely inflate near-source O_3, a bias noted in several evaluations.[15,60] In contrast, our PF simulations did not show elevated O_3 adjacent to burn areas, suggesting improved precursor balance or plume dispersion treatment. A further complication is the sheer chemical complexity of fire emissions: wildland fires emit hundreds of volatiles and oxygenated organic compounds, the majority of which are absent from standard gas-phase mechanisms. For instance, furans implicated in up to 10% of O_3 production within smoke plumes and major secondary-organic-aerosol precursors,[63] are typically excluded. With more than 500 distinct VOCs identified in biomass-burning plumes,[64−66] mechanism simplification is unavoidable, yet the consequences of these omissions for O_3 chemistry remain poorly quantified.

Prescribed burning was most prevalent during January−April, and our results showed substantial burning during May−September in several southeastern states. This seasonal timing is relevant for PF-O_3 formation because warmer temperatures and stronger solar radiation during summer generally favor photochemical O_3 production.[67,68] Consequently, PF occurring during warmer months may have a greater potential for O_3 formation per unit of precursor emissions than similar burns occurring under cooler conditions. For example, in 2019, Florida and South Carolina burned 13% and 29% more area per month, respectively, during October−December compared with May−September; nevertheless, the average PF-related O_3 concentrations were nearly identical between the two seasons.

The current analysis estimates higher short- and long-term all-cause mortality than previous studies[23,24] because we applied updated relative risk that shows a stronger association between PF-MDA8 O_3 exposure and mortality outcomes for both time scales. However, we did not consider the potential synergistic impacts of PF−$PM_{2.5}$ and PF-O_3 on long-term mortality, which tends to cause underestimation of the attributable deaths. Although O_3 is the same chemical species regardless of its source, the available epidemiological evidence indicates that wildland-fire-derived O_3 have associated with higher short-term mortality risks than all-source O_3, and similarly PF-O_3 exposure may occur in the presence of other fire-related pollutants and under distinct exposure conditions. Therefore, the estimated mortality burden should be interpreted cautiously, and further epidemiological studies

Downloaded from pubs.acs.org/ehnea2/article-pdf/doi/10.1021/envhealth.6c00221/6901887/envhealth.6c00221.pdf by UNIV OF LYNCHBURG, Zongrun Li on 01 November 2026

https://doi.org/10.1021/envhealth.6c00221
Environ. Health XXXX, XXX, XXX−XXX

are needed to establish robust source-specific long-term mortality risk estimates for PF-O_3. Using average daily county-level death counts in calculating short-term attributable deaths based on annual deaths and assuming that death rate does not change during JFMA could also result in underestimation.

There is frequent confusion over whether short-term and long-term mortality burdens from air pollution overlap or if short-term impacts are simply a subset of long-term effects. However, these burdens represent distinct outcomes based on different exposure timeframes and populations: short-term mortality refers to deaths occurring within hours to days of exposure, while long-term mortality represents deaths in future years resulting from cumulative exposure during the current year among individuals who did not die during that year.[69] Although long-term mortality is often estimated using current-year death data, this serves as a practical proxy for future deaths, assuming stable mortality rates and population continuity.[70] This methodological choice should not be misinterpreted as suggesting that long-term impacts occur within the same time frame as short-term effects. Therefore, short-term and long-term mortality burdens from PF-sourced air pollution should be treated as scientifically distinct and nonoverlapping.[41] In our previous study, we estimated 12 (8−17) and 31 (20−42) all-cause premature deaths attributable to short-term and long-term exposure to PF-MDA8 O_3 in Georgia in 2020.[23,24] In contrast, the present study yields higher estimates, with 43 (37−50) and 88 (54−122) deaths attributable to short-term and long-term exposure, respectively, for the same year.

Our study has some limitations. We used FINN data to obtain 1-km resolution hourly wildland burned-area information; however, FINN has limitations in capturing all of the burns because of cloud cover and temporal mismatches between prescribed burn activity and satellite overpass times.[71] Wildland-fire emission estimates from different inventories vary substantially.[18] For example, global biomass-burning organic carbon (OC) emissions derived from different inventories such as Global Fire Emissions Database (GFEDv3.1 and GFEDv4), FINNv1.5, Global Fire Assimilation System (GFASv1), Fire Energetics and Emissions Research (FEERv1.0), and Quick-Fire Emissions Data set (QFEDv2.4) differ by up to a factor of 3.8 on an annual average. In 2008, these data sets reported global OC emissions of 15.65, 13.76, 19.48, 18.22, 28.48, and 51.93 Tg C, respectively.[72] Similarly, other studies have quantified the high uncertainty in fire emission inventories.[73] The discrepancies may stem from differences in the number and detail of VOCs and NMVOCs included in each emission inventory. This study used BlueSky, which applies EFs for 190 VOC and NMVOC species and provides a detailed chemical profile based on US-specific fire studies. In contrast, GFEDv4 includes only 21 VOC species and QFEDv2.4 includes 9, and both rely on global EFs that lack the fuel-specific detail available in BlueSky. In addition to speciation, variations in input data, such as fire detection methods, burned-area estimates, and biomass consumption, also contribute to the divergent emission estimates across inventories.[74] These differences highlight the challenges in achieving consistency in fire emission inventories and the importance of carefully selecting and evaluating input data sets based on study goals and regional characteristics. Another key limitation is that PF-attributable O_3 cannot be directly validated because routine monitors measure only total ambient O_3 and cannot distinguish O_3 formed from PF emissions from that produced from anthropogenic, biogenic, wildfire, or background precursors. Additionally, applying wildland-fire O_3 risk estimates to prescribed fires introduces uncertainty due to differences in fire characteristics, copollutants, and exposure patterns. Future field measurements and PF-specific epidemiological studies are needed to improve PF-O_3 exposure and health-impact estimates.

Despite these limitations, this study provides valuable quantitative insights into the contribution of PF to O_3 pollution and offers important evidence for future epidemiological studies investigating the public-health impacts of PF in the southeastern US. In conclusion, PF-sourced O_3 contributes to ambient air pollution and a measurable mortality burden across the southeastern US, with substantial geographical and seasonal variation. As climate change increases fire-prone conditions and the use of prescribed burning potentially expands, integrated mitigation and adaptation strategies are needed to balance effective fire management with the protection of air quality and public health.

■ ASSOCIATED CONTENT

Data Availability Statement

The source data for the study are deposited in zenodo. All the data are freely available on https://zenodo.org/records/13380570. No custom code was used in this analysis. All code used is available upon request. Requests for materials should be addressed to M.T.O.

Supporting Information

The Supporting Information is available free of charge at https://pubs.acs.org/doi/10.1021/envhealth.6c00221.

Exposure assessment method (Figure S1), burn areas by year and season (Figure S2), maximum ozone impacts (Figures S3 and S4), ozone impacts by state (Figure S5), density scatterplots of observed vs modeled ozone (Figure S6), relative risks for short- and long-term mortality (Tables S1−S2), model performances (Tables S3 and S4), burn areas by state (Table S5), and seasonal ozone impacts by year (Tables S6−S13) (PDF)

■ AUTHOR INFORMATION

Corresponding Author

M. Talat Odman − *School of Civil and Environmental Engineering, Georgia Institute of Technology, Atlanta, Georgia 30332, United States*; Email: odman@gatech.edu

Authors

Kamal J. Maji − *Department of Public Health, Environments, and Society, London School of Hygiene & Tropical Medicine, London WC1H 9SH, U.K.; School of Civil and Environmental Engineering, Georgia Institute of Technology, Atlanta, Georgia 30332, United States*; orcid.org/0000-0001-7843-1204

Zongrun Li − *School of Civil and Environmental Engineering, Georgia Institute of Technology, Atlanta, Georgia 30332, United States*; orcid.org/0000-0003-4907-146X

Yongtao Hu − *School of Civil and Environmental Engineering, Georgia Institute of Technology, Atlanta, Georgia 30332, United States*

Downloaded from pubs.acs.org/ehnea2/article-pdf/doi/10.1021/envhealth.6c00221/6901887/envhealth.6c00221.pdf by UNIV OF LYNCHBURG, Zongrun Li on 01 November 2026

Jennifer D. Stowell − *School of Public Health, Boston University, Boston, Massachusetts 02118, United States*
Ambarish Vaidyanathan − *School of Civil and Environmental Engineering, Georgia Institute of Technology, Atlanta, Georgia 30332, United States*
Chad W. Milando − *School of Public Health, Boston University, Boston, Massachusetts 02118, United States*
Gregory A. Wellenius − *School of Public Health, Boston University, Boston, Massachusetts 02118, United States;* orcid.org/0000-0003-0427-7376
Patrick L. Kinney − *School of Public Health, Boston University, Boston, Massachusetts 02118, United States;* orcid.org/0000-0003-2801-1003
Armistead G. Russell − *School of Civil and Environmental Engineering, Georgia Institute of Technology, Atlanta, Georgia 30332, United States;* orcid.org/0000-0003-2027-8870

Complete contact information is available at: https://pubs.acs.org/10.1021/envhealth.6c00221

Author Contributions

K.J.M.: initiated the study, contributed to the study design, performed the analysis and interpretation of the data, writing—original draft and editing, visualization, software, formal analysis, data curation, conceptualization; Z.L.: initiated the study, performed the analysis, visualization, software, data curation, writing—review and editing; Y.H.: initiated the study, performed the analysis, software, data curation, writing—review and editing; J.D.S.: writing—review and editing, resources, conceptualization; C.W.M.: writing—review and editing; A.V.: writing—review and editing, resources; G.A.W. and P.L.K.: writing—review and editing, resources, funding acquisition; A.G.R.: contributed to the study design, writing—review and editing, resources, methodology, funding acquisition, conceptualization; M.T.O.: initiated the study, contributed to the study design, performed the analysis, writing—review and editing, resources, investigation, funding acquisition, conceptualization.

Funding

Research described in this article was conducted under Research Agreement No. 4988-RFA20-1A/21-11 between Georgia Institute of Technology and the Health Effects Institute (HEI), an organization jointly funded by the United States Environmental Protection Agency (EPA) (Assistance Award No. CR-83998101) and certain motor vehicle and engine manufacturers. In addition, K.J.M. and M.T.O. were supported in part by the Centers for Disease Control and Prevention (CDC) under Contract Number 75D30121P10715 to Georgia Institute of Technology. The views expressed in this article are those of the authors and do not necessarily reflect the views or policies of the CDC.

Notes

The authors declare no competing financial interest.

ACKNOWLEDGMENTS

Research cyberinfrastructure resources and services were provided by the Partnership for an Advanced Computing Environment (PACE) at the Georgia Institute of Technology, Atlanta, Georgia, USA.

REFERENCES

(1) Abatzoglou, J. T.; Williams, A. P. Impact of Anthropogenic Climate Change on Wildfire across Western US Forests. *Proc. Natl. Acad. Sci. U.S.A.* **2016**, *113* (42), 11770−11775.
(2) Wasserman, T. N.; Mueller, S. E. Climate Influences on Future Fire Severity: A Synthesis of Climate-Fire Interactions and Impacts on Fire Regimes, High-Severity Fire, and Forests in the Western United States. *Fire Ecol.* **2023**, *19* (1), 43.
(3) Coop, J. D.; Parks, S. A.; Stevens-Rumann, C. S.; Ritter, S. M.; Hoffman, C. M. Extreme Fire Spread Events and Area Burned under Recent and Future Climate in the Western USA. *Global Ecol. Biogeogr.* **2022**, *31* (10), 1949−1959.
(4) Ryan, K. C.; Knapp, E. E.; Varner, J. M. Prescribed Fire in North American Forests and Woodlands: History, Current Practice, and Challenges. *Front. Ecol. Environ.* **2013**, *11*, No. 120329, DOI: 10.1890/120329.
(5) Fernandes, P. M. Empirical Support for the Use of Prescribed Burning as a Fuel Treatment. *Curr. For. Rep.* **2015**, *1* (2), 118−127.
(6) Hunter, M. E.; Robles, M. D. Tamm Review: The Effects of Prescribed Fire on Wildfire Regimes and Impacts: A Framework for Comparison. *For. Ecol. Manage.* **2020**, *475*, No. 118435.
(7) Russell, A.; Fontana, N.; Hoecker, T.; Kamanu, A.; Majumder, R.; Stephens, J.; Young, A. M.; Cravens, A. E.; Giardina, C.; Hiers, K.; Littell, J.; Terando, A. A Fire-Use Decision Model to Improve the United States' Wildfire Management and Support Climate Change Adaptation. *Cell Rep. Sustainability* **2024**, *1* (6), No. 100125.
(8) Kelp, M.; Burke, M.; Qiu, M.; Higuera-Mendieta, I.; Liu, T.; Diffenbaugh, N. S. Effect of Recent Prescribed Burning and Land Management on Wildfire Burn Severity and Smoke Emissions in the Western United States. *AGU Adv.* **2025**, *6* (3), No. e1682, DOI: 10.1029/2025AV001682.
(9) Jose, E.; Agarwal, P.; Zhuang, J. A Data-Driven Analysis and Optimization of the Impact of Prescribed Fire Programs on Wildfire Risk in Different Regions of the USA. *Natl. Hazards* **2023**, *118* (1), 181−207.
(10) Environmental Protection Agency (EPA). Climate Change Indicators: Wildfires. https://www.epa.gov/climate-indicators/climate-change-indicators-wildfires (accessed October 03, 2025).
(11) Mark, A. M. National Prescribed Fire Use Survey Report. Technical Report, 2022.
(12) Afrin, S.; Garcia-Menendez, F. Potential Impacts of Prescribed Fire Smoke on Public Health and Socially Vulnerable Populations in a Southeastern U.S. State. *Sci. Total Environ.* **2021**, *794*, No. 148712.
(13) Schollaert, C. L.; Jung, J.; Wilkins, J.; Alvarado, E.; Baumgartner, J.; Brun, J.; Busch Isaksen, T.; Lydersen, J. M.; Marlier, M. E.; Marshall, J. D.; Masuda, Y. J.; Maxwell, C.; Tessum, C. W.; Wilson, K. N.; Wolff, N. H.; Spector, J. T. Quantifying the Smoke-Related Public Health Trade-Offs of Forest Management. *Nat. Sustainability* **2024**, *7* (2), 130−139.
(14) Jaffe, D. A.; O'Neill, S. M.; Larkin, N. K.; Holder, A. L.; Peterson, D. L.; Halofsky, J. E.; Rappold, A. G. Wildfire and Prescribed Burning Impacts on Air Quality in the United States. *J. Air Waste Manage. Assoc.* **2020**, *70* (6), 583−615.
(15) Baker, K. R.; Woody, M. C.; Tonnesen, G. S.; Hutzell, W.; Pye, H. O. T.; Beaver, M. R.; Pouliot, G.; Pierce, T. Contribution of Regional-Scale Fire Events to Ozone and PM2.5 Air Quality Estimated by Photochemical Modeling Approaches. *Atmos. Environ.* **2016**, *140*, 539−554.
(16) Chameides, W. L. The Photochemical Role of Tropospheric Nitrogen Oxides. *Geophys. Res. Lett.* **1978**, *5* (1), 17−20.
(17) Liu, S. C.; Kley, D.; McFarland, M.; Mahlman, J. D.; Levy, H. On the Origin of Tropospheric Ozone. *J. Geophys. Res.* **1980**, *85* (C12), 7546−7552.
(18) Wiedinmyer, C.; Akagi, S. K.; Yokelson, R. J.; Emmons, L. K.; Al-Saadi, J. A.; Orlando, J. J.; Soja, A. J. The Fire INventory from NCAR (FINN): A High Resolution Global Model to Estimate the Emissions from Open Burning. *Geosci. Model Dev.* **2011**, *4* (3), 625−641.

Downloaded from pubs.acs.org/ehnea2/article-pdf/doi/10.1021/envhealth.6c00221/6901887/envhealth.6c00221.pdf by UNIV OF LYNCHBURG, Zongrun Li on 01 November 2026

(19) Robinson, M. A.; Decker, Z. C. J.; Barsanti, K. C.; Coggon, M. M.; Flocke, F. M.; Franchin, A.; Fredrickson, C. D.; Gilman, J. B.; Gkatzelis, G. I.; Holmes, C. D.; Lamplugh, A.; Lavi, A.; Middlebrook, A. M.; Montzka, D. M.; Palm, B. B.; Peischl, J.; Pierce, B.; Schwantes, R. H.; Sekimoto, K.; Selimovic, V.; Tyndall, G. S.; Thornton, J. A.; Van Rooy, P.; Warneke, C.; Weinheimer, A. J.; Brown, S. S. Variability and Time of Day Dependence of Ozone Photochemistry in Western Wildfire Plumes. *Environ. Sci. Technol.* **2021**, *55* (15), 10280−10290.
(20) Yaro, V. S. O.; Bondé, L.; Bougma, P. C.; Sedgo, I.; Guuroh, R. T.; Gebremichael, A. W.; Neya, T.; Linstädter, A.; Ouédraogo, O. Greenhouse Gas Emission from Prescribed Fires Is Influenced by Vegetation Types in West African Savannas. *Sci. Rep.* **2024**, *14* (1), No. 23754.
(21) El Asmar, R.; Li, Z.; Tanner, D. J.; Hu, Y.; O'Neill, S.; Huey, L. G.; Odman, M. T.; Weber, R. J. A Multi-Site Passive Approach to Studying the Emissions and Evolution of Smoke from Prescribed Fires. *Atmos. Chem. Phys.* **2024**, *24* (22), 12749−12773.
(22) Raab, H.; Moyer, J.; Afrin, S.; Garcia-Menendez, F.; Ward-Caviness, C. K. Prescribed Fires, Smoke Exposure, and Hospital Utilization among Heart Failure Patients. *Environ. Health* **2023**, *22* (1), 86.
(23) Maji, K. J.; Li, Z.; Vaidyanathan, A.; Hu, Y.; Stowell, J. D.; Milando, C.; Wellenius, G.; Kinney, P. L.; Russell, A. G.; Odman, M. T. Estimated Impacts of Prescribed Fires on Air Quality and Premature Deaths in Georgia and Surrounding Areas in the US, 2015−2020. *Environ. Sci. Technol.* **2024**, *58* (28), 12343−12355.
(24) Maji, K. J.; Li, Z.; Hu, Y.; Vaidyanathan, A.; Stowell, J. D.; Milando, C.; Wellenius, G.; Kinney, P. L.; Russell, A. G.; Talat Odman, M. Prescribed Burn Related Increases of Population Exposure to PM2.5 and O3 Pollution in the Southeastern US over 2013−2020. *Environ. Int.* **2024**, *193*, No. 109101.
(25) Zhang, S.; Chen, Y.; Xiang, K.; He, L.; Lin, Y.; Khan, J.; Lai, K.; Zhang, J. J. Respiratory and Cardiovascular Effects of Ozone Modified by PM2.5: Evidence from a Panel Study and a Meta-Regression Analysis. *Environ. Sci. Technol.* **2026**, *60*, 23852.
(26) Earth Resources Observation and Science (EROS) Center. Landsat Enables Mapping of Fire Histories Across Florida. https://www.usgs.gov/news/landsat-enables-mapping-fire-histories-across-florida (accessed May 11, 2025).
(27) Cummins, K.; Noble, J.; Varner, J. M.; Robertson, K. M.; Hiers, J. K.; Nowell, H. K.; Simonson, E. The Southeastern U.S. Prescribed Fire Permit Database: Hot Spots and Hot Moments in Prescribed Fire across the Southeastern U.S.A. *Fire* **2023**, *6* (10), 372.
(28) Huang, R.; Zhang, X.; Chan, D.; Kondragunta, S.; Russell, A. G.; Odman, M. T. Burned Area Comparisons Between Prescribed Burning Permits in Southeastern United States and Two Satellite-Derived Products. *J. Geophys. Res.: Atmos.* **2018**, *123* (9), 4746−4757.
(29) Jonko, A.; Oliveto, J.; Beaty, T.; Atchley, A.; Battaglia, M. A.; Dickinson, M. B.; Gallagher, M. R.; Gilbert, A.; Godwin, D.; Kupfer, J. A.; Hiers, J. K.; Hoffman, C.; North, M.; Restaino, J.; Sieg, C.; Skowronski, N. How Will Future Climate Change Impact Prescribed Fire across the Contiguous United States? *npj Clim. Atmos. Sci.* **2024**, *7* (1), 96.
(30) Wiedinmyer, C.; Kimura, Y.; McDonald-Buller, E. C.; Emmons, L. K.; Buchholz, R. R.; Tang, W.; Seto, K.; Joseph, M. B.; Barsanti, K. C.; Carlton, A. G.; Yokelson, R. The Fire Inventory from NCAR Version 2.5: An Updated Global Fire Emissions Model for Climate and Chemistry Applications, 2023.
(31) Li, Z.; Maji, K. J.; Hu, Y.; Vaidyanathan, A.; O'Neill, S. M.; Odman, M. T.; Russell, A. G. An Analysis of Prescribed Fire Activities and Emissions in the Southeastern United States from 2013 to 2020. *Remote Sens.* **2023**, *15* (11), 2725.
(32) Wiedinmyer, C.; Kimura, Y.; McDonald-Buller, E. C.; Emmons, L. K.; Buchholz, R. R.; Tang, W.; Seto, K.; Joseph, M. B.; Barsanti, K. C.; Carlton, A. G.; Yokelson, R. The Fire Inventory from NCAR Version 2.5: An Updated Global Fire Emissions Model for Climate and Chemistry Applications. *Geosci. Model Dev.* **2023**, *16* (13), 3873−3891.
(33) Michael, R.; Mirabelli, M. C.; Vaidyanathan, A. Public Health Applications of Historical Smoke Forecasts: An Evaluation of Archived BlueSky Data for the Coterminous United States, 2015−2018. *Comput. Geosci.* **2023**, *171*, No. 105267.
(34) *Wildland Fire Smoke in the United States*; Peterson, D. L.; McCaffrey, S. M.; Patel-Weynand, T., Eds.; Springer International Publishing: Cham, 2022.
(35) Tran, H.; Polka, E.; Buonocore, J. J.; Roy, A.; Trask, B.; Hull, H.; Arunachalam, S. Air Quality and Health Impacts of Onshore Oil and Gas Flaring and Venting Activities Estimated Using Refined Satellite-Based Emissions. *Geohealth* **2024**, *8* (3), No. e938, DOI: 10.1029/2023GH000938.
(36) Senthilkumar, N.; Gilfether, M.; Metcalf, F.; Russell, A. G.; Mulholland, J. A.; Chang, H. H. Application of a Fusion Method for Gas and Particle Air Pollutants between Observational Data and Chemical Transport Model Simulations Over the Contiguous United States for 2005−2014. *Int. J. Environ. Res. Public Health* **2019**, *16* (18), 3314.
(37) Li, Z.; Lawal, A. S.; Zhang, B.; Maji, K. J.; Liu, P.; Hu, Y.; Russell, A. G.; Odman, M. T. A Generalized User-Friendly Method for Fusing Observational Data and Chemical Transport Model (GenFriberg V1.0: GF-1). *Environ. Modell. Software* **2026**, *197*, No. 106827.
(38) Friberg, M. D.; Zhai, X.; Holmes, H. A.; Chang, H. H.; Strickland, M. J.; Sarnat, S. E.; Tolbert, P. E.; Russell, A. G.; Mulholland, J. A. Method for Fusing Observational Data and Chemical Transport Model Simulations To Estimate Spatiotemporally Resolved Ambient Air Pollution. *Environ. Sci. Technol.* **2016**, *50* (7), 3695−3705.
(39) Baston, D. *Package Exactextractr*; R Foundation for Statistical Computing, 2021.
(40) Xu, X.; Lin, W.; Xu, W.; Jin, J.; Wang, Y.; Zhang, G.; Zhang, X.; Ma, Z.; Dong, Y.; Ma, Q.; Yu, D.; Li, Z.; Wang, D.; Zhao, H. Long-Term Changes of Regional Ozone in China: Implications for Human Health and Ecosystem Impacts. *Elem. Sci. Anth.* **2020**, *8*, No. e409, DOI: 10.1525/elementa.409.
(41) Xu, R.; Ye, T.; Huang, W.; Yue, X.; Morawska, L.; Abramson, M. J.; Chen, G.; Yu, P.; Liu, Y.; Yang, Z.; Zhang, Y.; Wu, Y.; Yu, W.; Wen, B.; Zhang, Y.; Hales, S.; Lavigne, E.; Saldiva, P. H. N.; Coelho, M. S. Z. S.; Matus, P.; Roye, D.; Klompmaker, J.; Mistry, M.; Breitner, S.; Zeka, A.; Raz, R.; Tong, S.; Johnston, F. H.; Schwartz, J.; Gasparrini, A.; Guo, Y.; Li, S. Global, Regional, and National Mortality Burden Attributable to Air Pollution from Landscape Fires: A Health Impact Assessment Study. *Lancet* **2024**, *404* (10470), 2447−2459.
(42) Ma, Y.; Zang, E.; Liu, Y.; Wei, J.; Lu, Y.; Krumholz, H. M.; Bell, M. L.; Chen, K. Long-Term Exposure to Wildland Fire Smoke PM $_{2.5}$ and Mortality in the Contiguous United States. *Proc. Natl. Acad. Sci. U.S.A.* **2024**, *121* (40), No. e2403960121, DOI: 10.1073/pnas.2403960121.
(43) Law, B. E.; Abatzoglou, J. T.; Schwalm, C. R.; Byrne, D.; Fann, N.; Nassikas, N. J. Anthropogenic Climate Change Contributes to Wildfire Particulate Matter and Related Mortality in the United States. *Commun. Earth Environ.* **2025**, *6* (1), 336.
(44) Pozzer, A.; Anenberg, S. C.; Dey, S.; Haines, A.; Lelieveld, J.; Chowdhury, S. Mortality Attributable to Ambient Air Pollution: A Review of Global Estimates. *Geohealth* **2023**, *7* (1), No. e711, DOI: 10.1029/2022GH000711.
(45) Alonso, C.; Gouveia, C. M.; Santos, J. A. Analysis of Tropospheric Ozone Concentration and Their Predictors in Mainland Portugal. *Atmos. Res.* **2025**, *314*, No. 107766.
(46) Chen, G.; Guo, Y.; Yue, X.; Xu, R.; Yu, W.; Ye, T.; Tong, S.; Gasparrini, A.; Bell, M. L.; Armstrong, B.; Schwartz, J.; Jaakkola, J. J. K.; Lavigne, E.; Saldiva, P. H. N.; Kan, H.; Royé, D.; Urban, A.; Vicedo-Cabrera, A. M.; Tobias, A.; Forsberg, B.; Sera, F.; Lei, Y.; Abramson, M. J.; Li, S.; Abrutzky, R.; Alahmad, B.; Ameling, C.; Åström, C.; Breitner, S.; Carrasco-Escobar, G.; Coêlho, M. de S. Z. S.; Colistro, V.; Correa, P. M.; Dang, T. N.; de'Donato, F.; Dung, D. Van.; Entezari, A.; Garcia, S. D. O.; Garland, R. M.; Goodman, P.;

Downloaded from pubs.acs.org/ehnea2/article-pdf/doi/10.1021/envhealth.6c00221/6901887/envhealth.6c00221.pdf by UNIV OF LYNCHBURG, Zongrun Li on 01 November 2026

Guo, Y. L.; Hashizume, M.; Holobaca, I.-H.; Honda, Y.; Houthuijs, D.; Hurtado-Díaz, M.; Íñiguez, C.; Katsouyanni, K.; Kim, H.; Kyselý, J.; Lee, W.; Maasikmets, M.; Madureira, J.; Mayvaneh, F.; Nunes, B.; Orru, H.; Ortega, N. V.; Overcenco, A.; Pan, S.-C.; Pascal, M.; Ragettli, M. S.; Rao, S.; Ryti, N. R. I.; Samoli, E.; Schneider, A.; Scovronick, N.; Seposo, X.; Stafoggia, M.; Valencia, C. D. C.; Zanobetti, A.; Zeka, A. All-Cause, Cardiovascular, and Respiratory Mortality and Wildfire-Related Ozone: A Multicountry Two-Stage Time Series Analysis. *Lancet Planet. Health* **2024**, *8* (7), e452−e462.

(47) *Mortality Rates by Causes of Death and Life Expectancy by County, Race, and Ethnicity 2000−2019* Institute for Health Metrics and Evaluation (IHME): Seattle, United States; 2023.

(48) National Cancer Institute. Download U.S. County Population Data - 1969−2023. https://seer.cancer.gov/popdata/download.html (accessed March 10, 2025).

(49) Emery, C.; Liu, Z.; Russell, A. G.; Odman, M. T.; Yarwood, G.; Kumar, N. Recommendations on Statistics and Benchmarks to Assess Photochemical Model Performance. *J. Air Waste Manage. Assoc.* **2017**, *67* (5), 582−598.

(50) Poulter, B.; Freeborn, P. H.; Jolly, W. M.; Varner, J. M. COVID-19 Lockdowns Drive Decline in Active Fires in Southeastern United States. *Proc. Natl. Acad. Sci. U.S.A.* **2021**, *118* (43), No. e2105666118, DOI: 10.1073/pnas.2105666118.

(51) He, H.; Liang, X.-Z.; Sun, C.; Tao, Z.; Tong, D. Q. The Long-Term Trend and Production Sensitivity Change in the US Ozone Pollution from Observations and Model Simulations. *Atmos. Chem. Phys.* **2020**, *20* (5), 3191−3208.

(52) Gutowski, W. J.; Ullrich, P. A.; Hall, A.; Leung, L. R.; O'Brien, T. A.; Patricola, C. M.; Arritt, R. W.; Bukovsky, M. S.; Calvin, K. V.; Feng, Z.; Jones, A. D.; Kooperman, G. J.; Monier, E.; Pritchard, M. S.; Pryor, S. C.; Qian, Y.; Rhoades, A. M.; Roberts, A. F.; Sakaguchi, K.; Urban, N.; Zarzycki, C. The Ongoing Need for High-Resolution Regional Climate Models: Process Understanding and Stakeholder Information. *Bull. Am. Meteorol. Soc.* **2020**, *101* (5), E664−E683.

(53) Yin, L.; Bai, B.; Zhang, B.; Zhu, Q.; Di, Q.; Requia, W. J.; Schwartz, J. D.; Shi, L.; Liu, P. Regional-Specific Trends of PM2.5 and O3 Temperature Sensitivity in the United States. *NPJ. Clim. Atmos. Sci.* **2025**, *8* (1), 12.

(54) Wang, Y.; Bastien, L.; Wang, Y.; Jin, L.; Harley, R. Temperature and Stagnation Effects on Ozone Sensitivity to NOx and VOC: An Adjoint Modeling Study in Central California, 2025.

(55) Larkin, N. K.; O'Neill, S. M.; Solomon, R.; Raffuse, S.; Strand, T.; Sullivan, D. C.; Krull, C.; Rorig, M.; Peterson, J.; Ferguson, S. A. The BlueSky Smoke Modeling Framework. *Int. J. Wildland Fire* **2009**, *18* (8), 906.

(56) Rappold, A. G.; Reyes, J.; Pouliot, G.; Cascio, W. E.; Diaz-Sanchez, D. Community Vulnerability to Health Impacts of Wildland Fire Smoke Exposure. *Environ. Sci. Technol.* **2017**, *51* (12), 6674−6682.

(57) Fann, N.; Alman, B.; Broome, R. A.; Morgan, G. G.; Johnston, F. H.; Pouliot, G.; Rappold, A. G. The Health Impacts and Economic Value of Wildland Fire Episodes in the U.S.: 2008−2012. *Sci. Total Environ.* **2018**, *610−611*, 802−809.

(58) Val Martin, M.; Heald, C. L.; Lamarque, J.-F.; Tilmes, S.; Emmons, L. K.; Schichtel, B. A. How Emissions, Climate, and Land Use Change Will Impact Mid-Century Air Quality over the United States: A Focus on Effects at National Parks. *Atmos. Chem. Phys.* **2015**, *15* (5), 2805−2823.

(59) Reddington, C. L.; Conibear, L.; Robinson, S.; Knote, C.; Arnold, S. R.; Spracklen, D. V. Air Pollution From Forest and Vegetation Fires in Southeast Asia Disproportionately Impacts the Poor. *Geohealth* **2021**, *5* (9), No. e418, DOI: 10.1029/2021GH000418.

(60) Jaffe, D. A.; Wigder, N. L. Ozone Production from Wildfires: A Critical Review. *Atmos. Environ.* **2012**, *51*, 1−10.

(61) Jin, X.; Fiore, A. M.; Murray, L. T.; Valin, L. C.; Lamsal, L. N.; Duncan, B.; Folkert Boersma, K.; De Smedt, I.; Abad, G. G.; Chance, K.; Tonnesen, G. S. Evaluating a Space-Based Indicator of Surface Ozone-NOx-VOC Sensitivity Over Midlatitude Source Regions and Application to Decadal Trends. *J. Geophys. Res.: Atmos.* **2017**, *122* (19), No. e1, DOI: 10.1002/2017JD026720.

(62) Meng, X.; Pang, K.; Yin, Z.; Xiang, X. Grid-Based Spatiotemporal Modeling of Ambient Ozone to Assess Human Exposure Using Environmental Big Data. *Atmos. Pollut. Res.* **2021**, *12* (12), No. 101216.

(63) Coggon, M. M.; Lim, C. Y.; Koss, A. R.; Sekimoto, K.; Yuan, B.; Gilman, J. B.; Hagan, D. H.; Selimovic, V.; Zarzana, K. J.; Brown, S. S.; Roberts, J. M.; Müller, M.; Yokelson, R.; Wisthaler, A.; Krechmer, J. E.; Jimenez, J. L.; Cappa, C.; Kroll, J. H.; de Gouw, J.; Warneke, C. OH Chemistry of Non-Methane Organic Gases (NMOGs) Emitted from Laboratory and Ambient Biomass Burning Smoke: Evaluating the Influence of Furans and Oxygenated Aromatics on Ozone and Secondary NMOG Formation. *Atmos. Chem. Phys.* **2019**, *19* (23), 14875−14899.

(64) Hatch, L. E.; Yokelson, R. J.; Stockwell, C. E.; Veres, P. R.; Simpson, I. J.; Blake, D. R.; Orlando, J. J.; Barsanti, K. C. Multi-Instrument Comparison and Compilation of Non-Methane Organic Gas Emissions from Biomass Burning and Implications for Smoke-Derived Secondary Organic Aerosol Precursors. *Atmos. Chem. Phys.* **2017**, *17* (2), 1471−1489.

(65) Wentworth, G. R.; Aklilu, Y.; Landis, M. S.; Hsu, Y.-M. Impacts of a Large Boreal Wildfire on Ground Level Atmospheric Concentrations of PAHs, VOCs and Ozone. *Atmos. Environ.* **2018**, *178*, 19−30.

(66) Kumar, V.; Chandra, B. P.; Sinha, V. Large Unexplained Suite of Chemically Reactive Compounds Present in Ambient Air Due to Biomass Fires. *Sci. Rep.* **2018**, *8* (1), No. 626.

(67) Nguyen, D.-H.; Lin, C.; Vu, C.-T.; Cheruiyot, N. K.; Nguyen, M. K.; Le, T. H.; Lukkhasorn, W.; Vo, T.-D.-H.; Bui, X.-T. Tropospheric Ozone and NO: A Review of Worldwide Variation and Meteorological Influences. *Environ. Technol. Innov.* **2022**, *28*, No. 102809.

(68) Li, S.; Wang, H.; Lu, X. Anthropogenic Emission Controls Reduce Summertime Ozone−Temperature Sensitivity in the United States. *Atmos. Chem. Phys.* **2025**, *25* (4), 2725−2743.

(69) Liu, J. C.; Pereira, G.; Uhl, S. A.; Bravo, M. A.; Bell, M. L. A Systematic Review of the Physical Health Impacts from Non-Occupational Exposure to Wildfire Smoke. *Environ. Res.* **2015**, *136*, 120−132.

(70) Cohen, A. J.; Brauer, M.; Burnett, R.; Anderson, H. R.; Frostad, J.; Estep, K.; Balakrishnan, K.; Brunekreef, B.; Dandona, L.; Dandona, R.; Feigin, V.; Freedman, G.; Hubbell, B.; Jobling, A.; Kan, H.; Knibbs, L.; Liu, Y.; Martin, R.; Morawska, L.; Pope, C. A.; Shin, H.; Straif, K.; Shaddick, G.; Thomas, M.; van Dingenen, R.; van Donkelaar, A.; Vos, T.; Murray, C. J. L.; Forouzanfar, M. H. Estimates and 25-Year Trends of the Global Burden of Disease Attributable to Ambient Air Pollution: An Analysis of Data from the Global Burden of Diseases Study 2015. *Lancet* **2017**, *389* (10082), 1907−1918.

(71) Nowell, H. K.; Holmes, C. D.; Robertson, K.; Teske, C.; Hiers, J. K. A New Picture of Fire Extent, Variability, and Drought Interaction in Prescribed Fire Landscapes: Insights From Florida Government Records. *Geophys. Res. Lett.* **2018**, *45* (15), 7874−7884.

(72) Pan, X.; Ichoku, C.; Chin, M.; Bian, H.; Darmenov, A.; Colarco, P.; Ellison, L.; Kucsera, T.; da Silva, A.; Wang, J.; Oda, T.; Cui, G. Six Global Biomass Burning Emission Datasets: Intercomparison and Application in One Global Aerosol Model. *Atmos. Chem. Phys.* **2020**, *20* (2), 969−994.

(73) Anderson, K.; Chen, J.; Englefield, P.; Griffin, D.; Makar, P. A.; Thompson, D. The Global Forest Fire Emissions Prediction System Version 1.0. *Geosci. Model Dev.* **2024**, *17* (21), 7713−7749.

(74) Jin, L.; Permar, W.; Selimovic, V.; Ketcherside, D.; Yokelson, R. J.; Hornbrook, R. S.; Apel, E. C.; Ku, I.-T.; Collett, J. L., Jr.; Sullivan, A. P.; Jaffe, D. A.; Pierce, J. R.; Fried, A.; Coggon, M. M.; Gkatzelis, G. I.; Warneke, C.; Fischer, E. V.; Hu, L. Constraining Emissions of Volatile Organic Compounds from Western US Wildfires with WE-CAN and FIREX-AQ Airborne Observations. *Atmos. Chem. Phys.* **2023**, *23* (10), 5969−5991.

Downloaded from pubs.acs.org/ehnea2/article-pdf/doi/10.1021/envhealth.6c00221/6901887/envhealth.6c00221.pdf by UNIV OF LYNCHBURG, Zongrun Li on 01 November 2026